AlphaB-crystallin regulates remyelination after peripheral nerve injury

Erin-Mai F. Lim[a,b], Stan T. Nakanishi[c], Vahid Hoghooghi[a,b], Shane E. A. Eaton[a,b], Alexandra L. Palmer[a,b], Ariana Frederick[b,d], Jo A. Stratton[b,e], Morgan G. Stykel[a,b], Patrick J. Whelan[b,e,f], Douglas W. Zochodne[g], Jeffrey Biernaskie[b,e], and Shalina S. Ousman[b,d,h,1]

[a]Department of Neuroscience, University of Calgary, Calgary, AB, Canada, T2N 4N1; [b]Hotchkiss Brain Institute, Calgary, AB, Canada, T2N 4N1; [c]Department of Biology, University of Hawai'i at Hilo, Hilo, HI 96720; [d]Department of Clinical Neurosciences, University of Calgary, Calgary, AB, Canada, T2N 4N1; [e]Department of Comparative Biology and Experimental Medicine, University of Calgary, Calgary, AB, Canada, T2N 4N1; [f]Department of Physiology and Pharmacology, University of Calgary, Calgary, AB, Canada, T2N 4N1; [g]Department of Medicine, University of Alberta, Edmonton, AB, Canada, T6G 2B7; and [h]Department of Cell Biology & Anatomy, University of Calgary, Calgary, AB, Canada, T2N 4N1

Edited by Tomas G. M. Hokfelt, Karolinska Institutet, Stockholm, Sweden, and approved December 30, 2016 (received for review July 22, 2016)

AlphaB-crystallin (αBC) is a small heat shock protein that is constitutively expressed by peripheral nervous system (PNS) axons and Schwann cells. To determine what role this crystallin plays after peripheral nerve damage, we found that loss of αBC impaired remyelination, which correlated with a reduced presence of myelinating Schwann cells and increased numbers of nonmyelinating Schwann cells. The heat shock protein also seems to regulate the cross-talk between Schwann cells and axons, because expected changes in neuregulin levels and ErbB2 receptor expression after PNS injury were disrupted in the absence of αBC. Such dysregulations led to defects in conduction velocity and motor and sensory functions that could be rescued with therapeutic application of the heat shock protein in vivo. Altogether, these findings show that αBC plays an important role in regulating Wallerian degeneration and remyelination after PNS injury.

peripheral nerve injury | remyelination | Schwann cells | alphaB-crystallin | Wallerian degeneration

The robust regenerative capacity of the damaged peripheral nervous system (PNS) is partly determined by cellular and molecular events that occur in the nerve segment distal to the injury site (1). For instance, during Wallerian degeneration, influx of calcium into the damaged nerve within 12–24 h of PNS injury activates proteases (2) that result in cytoskeletal breakdown and subsequent disintegration of the axon membrane. This axon degeneration is then followed by breakdown of the myelin sheath within 2 d (3). Schwann cells, the glial cells that characterize the PNS, subsequently undergo a number of reactive physiological changes that benefit the damaged axon. Within 48 h of peripheral nerve damage, myelinating Schwann cells decrease their expression of myelin proteins, such as myelin basic protein (MBP), peripheral myelin protein 22, and protein 0 (P0) (4), and along with their nonmyelinating counterparts, revert to a nonmyelinating phenotype (4). At ∼3–4 d postinjury, the dedifferentiated Schwann cells proliferate (5–7) and align within the basal lamina to form bands of Büngner that provide a structural and trophic supportive substrate for regenerating axons. These Schwann cells secrete neurotrophic factors that provide trophic sustenance to damaged neurons until they reestablish contact with their targets (8) and produce extracellular matrix molecules that encourage and guide outgrowing axons (9), whereas secretion of chemokines is thought to mediate the infiltration of blood-derived macrophages, which along with Schwann cells, phagocytose myelin debris and its associated axon growth inhibitors (9). Finally, based on the level of neuregulin 1 Types I and III on Schwann cells and axons, respectively, and their binding to their cognate receptors ErbB2/ErbB3 on Schwann cells, these glia will revert to a myelinating or ensheathing phenotype on contact with regrowing axons (10). Altogether, these morphological and physiological changes in Schwann cells create an environment that encourages long-distance axon growth.

In humans, however, regrowth of damaged peripheral nerves is often incomplete, which can result in partial or complete loss of motor, sensory, and autonomic functions; neuropathic pain; or inappropriate sensations (11). This insubstantial regrowth of damaged peripheral axons in humans is attributed to a variety of factors: (*i*) the slow rate of axon regrowth (∼1 mm/d); (*ii*) the often far distances of the injury site from the target; (*iii*) the severity of the injury (transection vs. crush, where there is a complete loss of connective tissue in the former); (*iv*) lack of selective axon–target reconnection; (*v*) nerve gap distance, where gaps longer than 4 cm preclude recovery almost completely; (*vi*) an inability of denervated muscles to accept reinnervation; (*vii*) extensive associated injuries, such as vascular disruptions; (*viii*) older age of the individual (12); and (*ix*) deterioration of the growth-supportive abilities of Schwann cells (13–15). We are interested in understanding what regulates the beneficial processes of Schwann cells so as to improve regeneration and functional recovery in humans after damage to peripheral axons.

Schwann cells (16, 17) as well as cell bodies and axons of peripheral neurons (18) constitutively express a small heat shock protein called alphaB-crystallin (αBC), but its function in the uninjured and damaged PNS is unknown. αBC (also called CRYAB or HSPB5) is a 22-kDa protein that possesses a number of beneficial and protective properties, including chaperoning

Significance

Regeneration and full behavioral recovery after injury to human peripheral nerves are often incomplete. To identify factors that could improve this situation, we focused on alphaB-crystallin (αBC), a small heat shock protein that has been associated with survival and differentiation of glial cells as well as neuroprotection in the central nervous system. We report that αBC, which is expressed by both peripheral axons and Schwann cells, is important for remyelination of damaged, peripheral axons in mice. Its absence resulted in thinner myelin sheaths and fewer myelinating Schwann cells. As a consequence, nerve conduction and sensory and motor behaviors were negatively impacted. Our work, therefore, suggests that administration of αBC can improve the regenerative capacity of the peripheral nervous system.

Author contributions: E.-M.F.L., and S.S.O. designed research; P.J.W., D.W.Z., and J.B. advised on experimental design; E.-M.F.L., S.T.N., V.H., S.E.A.E., A.L.P., A.F., J.A.S., and M.G.S. performed research; E.-M.F.L., S.T.N., and S.E.A.E. analyzed data; and E.-M.F.L. and S.S.O. wrote the paper.

The authors declare no conflict of interest.

This article is a PNAS Direct Submission.

Freely available online through the PNAS open access option.

See Commentary on page 2103.

[1]To whom correspondence should be addressed. Email: sousman@ucalgary.ca.

This article contains supporting information online at www.pnas.org/lookup/suppl/doi:10.1073/pnas.1612136114/-/DCSupplemental.

(19, 20), prosurvival (21), immunosuppression (22, 23), and antineurotoxic (24) abilities. With respect to the PNS, D'Antonio et al. (16) found that αBC was expressed late during PNS development and that the heat shock protein was highly expressed in mature peripheral nerves, with equal levels in both myelinating and nonmyelinating Schwann cells. Furthermore, expression of αBC was up-regulated during PNS myelination and down-regulated in cut rat sciatic nerves (16). Recently, Klopstein et al. (25) showed that αBC was therapeutic after spinal cord contusion injury in mice, whereby treatment with recombinant human (rhu)-CRYAB postdamage resulted in reduced secondary tissue damage and greater locomotor recovery. In light of its expression in the PNS together with its numerous beneficial and protective functions, we investigated whether αBC influenced the injury-related events that occur after PNS damage. Here, we show that αBC is important for remyelination of regenerated peripheral axons by regulating the conversion of dedifferentiated Schwann cells back to a myelinating phenotype. We also show that the heat shock protein contributes to the early communication between Schwann cells and damaged axons to signal that an injury has occurred. Finally, exogenous application of αBC may have therapeutic capabilities by promoting remyelination and functional recovery after PNS injury.

Results

αBC Is Expressed by Schwann Cells and Axons, and Its Level and Expression Are Decreased in Sciatic Nerves After Crush Injury. Previous work has shown that αBC is expressed constitutively in peripheral axons and Schwann cells from rat (16–18). We thus first checked if the heat shock protein was expressed in peripheral nerves from mice. High levels of αBC were evident in sciatic nerves from naïve 129S6 wild-type (WT) mice (Fig. 1*A*) with colocalization to MBP-positive (+) Schwann cells and neurofilament H (NF-H)-stained axons (Fig. 1*B*). No localization of the heat shock protein was seen in glial fibrillary acidic protein^{+} (GFAP^{+}) nonmyelinating Schwann cells, F4/80^{+} macrophages, or Asma^{+} fibroblasts (Fig. 1*B* and Fig. S1). As expected, the crystallin was absent in nerves from αBC$^{-/-}$ animals (Fig. 1*A*). We next evaluated whether the levels of the heat shock protein were altered after sciatic nerve crush. Within 24 h of damage in WT animals, there was a significant decrease in the amount of αBC in the nerve segment distal to the crush site (Fig. 1*C*). This reduction was sustained until ∼28 d postinjury, after which the levels started to rebound relative to the lowest expression seen at day 21 after crush (Fig. 1*C*). These data were confirmed at the histological level, where a reduction in αBC immunostaining was evident at 7 d after crush injury compared with intact nerves (Fig. 1 *B* and *D* and Fig. S1).

Sensory and Motor Behaviors Are Impaired in αBC$^{-/-}$ Mice After Sciatic Nerve Crush. To assess whether removal of αBC impacted functional recovery, we evaluated motor and sensory behaviors associated with sciatic nerve regeneration at 28 d postcrush, a time point when regeneration is robust in WT mice (26) and when the levels of αBC were rebounding in the crushed sciatic nerves of WT mice (Fig. 1*C*). To obtain an overall impression of effects on gait dynamics, the DigiGait Imaging System was used to assess parameters associated with regeneration, such as swing, braking, propulsion, stance, and paw area (Fig. S2 and Table S1). We first determined that the speed of the treadmill that allowed for proper gait dynamics (27) in our 129S6 strain of mice was 15 cm/s. We then compared movement properties in uninjured 2-mo-old WT and αBC$^{-/-}$ animals (age at which crush injury was performed) to assess whether there were any preexisting differences in walking dynamics. No difference in swing duration (Fig. 2*A*), stance duration (Fig. 2*B*), braking duration (Fig. 2*C*), propulsion duration (Fig. 2*D*), or paw area (Fig. 2*E*) was seen between the two uninjured, naïve groups (Table S2). The same mice were then retested 28 d after a crush injury. In WT animals, the gait parameters had recovered and were comparable with those of the naïve WT group. In injured αBC$^{-/-}$ mice, however, braking duration, propulsion duration, paw area, and stance duration were significantly lower

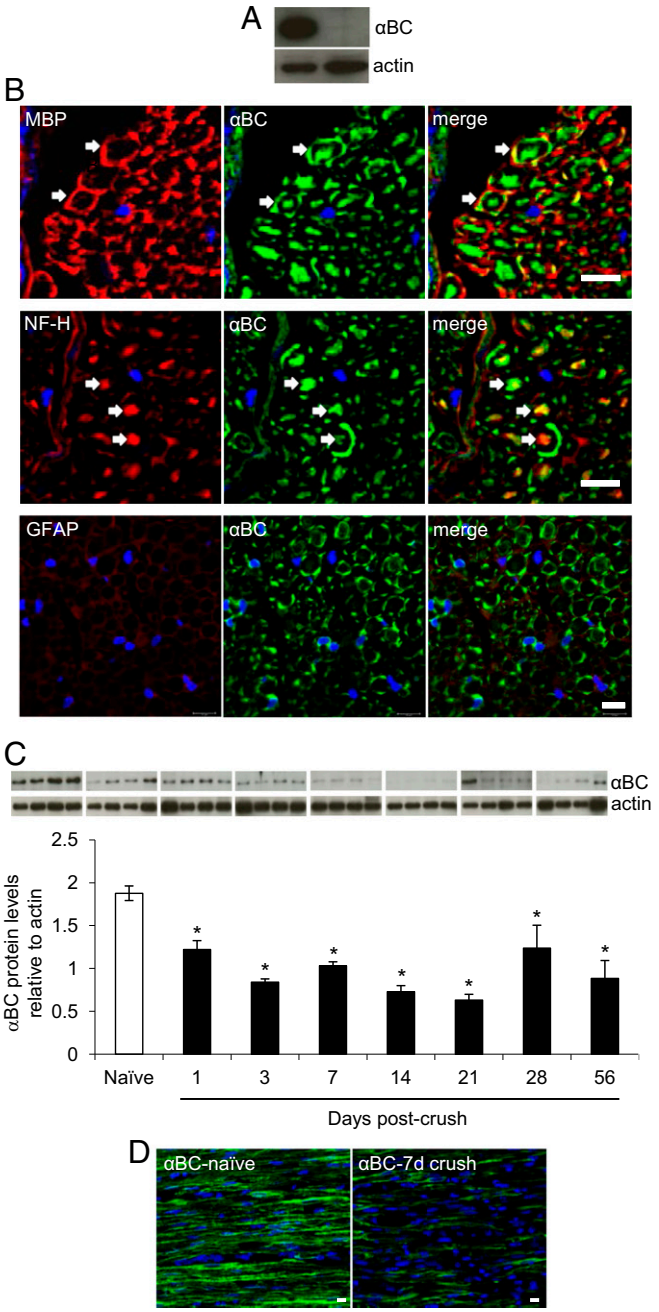

Fig. 1. Expression of αBC in sciatic nerves before and after crush injury. (*A*) Western blot image showing expression levels of αBC in sciatic nerves from naïve 129SVE WT and αBC$^{-/-}$ mice. (*B*) Immunohistochemical staining for αBC, MBP, NF-H, GFAP, and DAPI in cross-sections of sciatic nerves from WT naïve mice. (Magnification: 40×; scale bar: 10 μm.) (*C*) Western blot image and ImageJ quantification of the levels of αBC and actin in sciatic nerves from WT naïve animals at 1, 3, 7, 14, 21, 28, and 56 d postcrush (representative of two experiments, with each bar consisting of four animals per time point). Data were analyzed using the independent *t* test comparison with the naïve time point and are shown as means ± SEM. $^{*}P < 0.05$. (*D*) Immunohistochemical staining for αBC in longitudinal sections of naïve and 7-d crushed WT nerves. (Scale bar: 10 μm.)

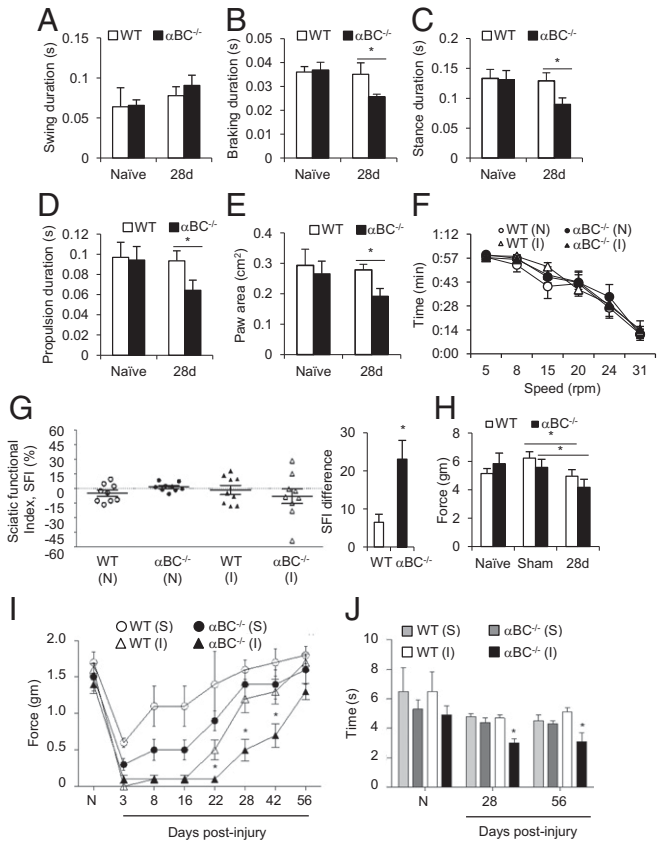

Fig. 2. Sensory and motor behaviors in WT and αBC$^{-/-}$ mice after sciatic nerve crush. DigiGait analysis of (*A*) swing duration, (*B*) stance duration, (*C*) braking duration, (*D*) propulsion duration, and (*E*) paw area in naïve and 28-d postcrushed WT (white bars) and αBC$^{-/-}$ (black bars) mice (representative of two experiments; n = 3–5 mice per group). (*F*) RotaRod test performed on naïve (N; white and black circles) and 28-d injured (I; white and black triangles) WT (white symbols) and αBC$^{-/-}$ (black symbols) mice (one experiment; n = 9–10 animals per group). (*G*) SFI examination and SFI difference in WT (circles and white bar) and αBC$^{-/-}$ (triangles and black bar) mice before (N) and 28 d after crush injury (I; representative of two experiments; n = 9–10 mice per group). (*H*) Dynamic plantar test in naïve, sham, and 28-d injured WT (white bars) and αBC$^{-/-}$ (black bars) mice (one experiment; n = 9–10 animals per group). (*I*) von Frey Hair examination in sham (S) and 28-d injured (I) WT (circles) and αBC$^{-/-}$ (triangles) animals (representative of two experiments; n = 7–10 mice per group). (*J*) Hargreaves test in naïve (N) and injured WT and αBC$^{-/-}$ mice at 28 and 56 d after sham (S) and injury (I) surgeries (representative of two experiments; n = 7–10 mice per group). All data were analyzed using two-way repeated measures ANOVA and represent mean ± SEM. *$P < 0.05$.

relative to their WT counterparts (Fig. 2 *B–E* and Table S2), whereas swing duration had recovered (Fig. 2*A* and Table S2). These results indicate that overall functional recovery was impaired in the injured αBC$^{-/-}$ animals.

Reduction in paw area, braking duration, and propulsion duration is suggestive of sensory and motor impairment (28). We, therefore, validated the DigiGait findings using classical motor (rotarod and walking track) and sensory (Hargreaves, Dynamic Plantar, and von Frey Hair) behavioral tests. In the rotarod examination, which measures motor coordination, no difference was observed between naïve and 28-d postinjured WT and αBC$^{-/-}$ animals (Fig. 2*F*). However, in the walking track test, which analyzes walking patterns to assess sensory and motor functionality during locomotion, WT animals showed some abnormality in walking at 28 d postcrush as evidenced by the sciatic functional index (SFI) scores that showed a range difference of 6.50 ± 2.12 (Fig. 2*G*). However, an even greater statistically significant exaggeration in walking impairment was seen in the αBC$^{-/-}$ mice, which displayed an SFI difference of 23.10 ± 4.90 (Fig. 2*G*). Both uninjured naïve WT and αBC$^{-/-}$ mice displayed SFI values close to zero, which indicate that there was no developmental abnormality in gait in the null animals (Fig. 2*G*).

Effects on sensory behavior were then assessed with the Dynamic Plantar, Hargreaves, and von Frey Hair tests. For the Dynamic Plantar examination, which is a measure of mechanical sensitivity, although differences were observed between the sham and injured groups for both genotypes, no difference was evident between WT and null cohorts at 28 d after injury (Fig. 2*H*). We then used the von Frey Hair test, which is another but more sensitive examination for mechanical sensitivity. Here, although both WT and αBC$^{-/-}$ mice displayed increased sensitivity at the earlier time points postinjury (3, 8, and 16 d), WT mice began to recover by day 22 to preinjury values and fully recovered by day 28. However, αBC$^{-/-}$ mice only started to recover by day 28 and remained sensitive to lower forces until 56 d postcrush (Fig. 2*I*). Finally, in the Hargreaves test, which measures for sensitivity to radiant heat, no difference in paw withdrawal was observed between uninjured WT and αBC$^{-/-}$ animals. At 28 and 56 d postcrush, however, the injured null animals displayed increased sensitivity compared with their WT cohorts as seen by the reduced time in limb withdrawal (Fig. 2*J*). Altogether, the functional examinations revealed that the αBC$^{-/-}$ animals displayed impairment in motor and sensory behaviors compared with their WT cohorts after sciatic nerve crush injury.

Conduction Velocity Is Reduced in Sciatic Nerves from αBC$^{-/-}$ Mice After Sciatic Nerve Crush Injury. We then evaluated whether the behavioral deficits seen in the injured αBC$^{-/-}$ mice were related to impairment in nerve conduction. We first assessed the normalized distal motor latency of the sciatic–dorsal interosseus motor system in naïve and injured WT and αBC$^{-/-}$ animals. No difference in normalized latency was seen between naïve, uninjured WT and null animals at a fixed distance (Fig. 3 *A–C*). Twenty-eight days after crush injury, αBC$^{-/-}$ mice displayed a greater latency (Fig. 3*D*) compared with the WT cohort over a similar distance (Fig. 3*E*). When the normalized latency was calculated, the null cohort displayed a reduction compared with injured WT controls (Fig. 3 *F* and *G*), indicating that recovery was less robust in injured αBC$^{-/-}$ animals.

To determine whether the impairment in normalized latency in αBC$^{-/-}$ mice was specifically related to axonal electrophysiological properties, independent of neuromuscular junction transmission, we measured the motor nerve conduction velocity (MNCV). We found that null mice displayed lower MNCV at 28 d postcrush compared with the injured WT cohort (Fig. 3*H*). This effect was specific to the injury process and was not caused by an underlying genetically mediated influence, because no difference in MNCV was seen in naïve or sham WT and αBC$^{-/-}$ animals (Fig. 3*H*). Furthermore, it appeared that the MNCV was specifically altered and not the number of fibers being recruited during the electrical transmission, because the amplitude of the compound motor action potential was similar between WT and αBC$^{-/-}$ animals both before and after injury (Fig. 3 *I* and *J*). Collectively, these results indicate that there was a delay in the recovery of normal electrophysiological properties of motor axons in null mice after crush injury.

αBC Positively Modulates Remyelination After Sciatic Nerve Crush. Because myelination and axonal integrity play a critical role in the electrophysiological properties of axons as well as motor and sensory behaviors, we assessed whether the defects seen in these parameters (Figs. 2 and 3) were because structural evidence of remyelination or axonal growth was different between WT and αBC$^{-/-}$ animals at 28 d after injury, a time when these two events

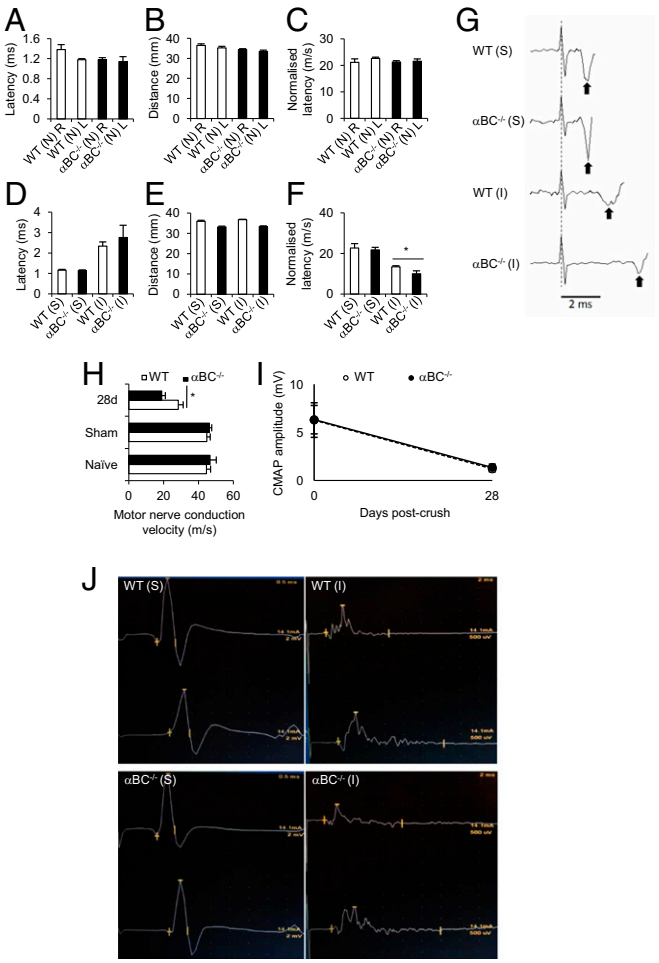

Fig. 3. Electrophysiological properties of motor axons in sciatic nerves of WT and $\alpha BC^{-/-}$ mice after crush injury. (*A* and *D*) Latency, (*B* and *E*) distance, and (*C* and *F*) normalized latency in (*A–C*) naïve (N) and (*D–F*) 28-d post-surgery sham (S) and injured (I) WT (white bars) and $\alpha BC^{-/-}$ (black bars) mice after a single-point stimulation of the sciatic nerve (one experiment; $n = 5$ per group). $^*P < 0.05$ (two-way ANOVA). (*G*) An example of the raw data for the normalized latency reflecting mean data represented in *F*. The dotted line indicates the stimulus artifact, and the black arrows indicate the first poststimulus voltage deflections associated with the arrival of motor volley near the recording electrode. The latency was measured from the dashed line to the arrows. Trace is an average of 20 individual stimulus trials. (*H*) MNCV in naïve, sham, and 28-d postdamaged WT (white bars) and $\alpha BC^{-/-}$ (black bars) animals (representative of two experiments; $n = 9–10$ mice per arm). $^*P < 0.05$ (two-way repeated measures ANOVA). (*I*) CMAP amplitude of sham (0) and 28-d injured WT and $\alpha BC^{-/-}$ mice. (*J*) Representative traces of the raw data from which the CMAP data and MNCV were derived in sham (S) and 28-d injured (I) WT and $\alpha BC^{-/-}$ mice.

are robust in injured WT animals (26). For remyelination, we quantified g ratios ranging from 0.4 to greater than 0.85, where 0.7 is the optimal myelin thickness for nerve conduction (29). Compared with injured WT nerves, we found that the g ratios in crushed $\alpha BC^{-/-}$ mice were skewed toward higher values (Fig. 4*B*), which indicated that remyelination was impaired. Specifically, the frequency of low g-ratio profiles (axons with thick myelin sheaths) was significantly reduced in $\alpha BC^{-/-}$ animals, whereas a marked increase in the frequency of high g-ratio values (indicative of axons with thin myelin sheaths) was greater in these animals compared with their WT cohort (Fig. 4*B*). Importantly, the defect in remyelination exhibited by the $\alpha BC^{-/-}$ mice was not caused by preexisting differences in the naïve, uninjured mice but rather, was related to the injury paradigm, because the g-ratio profiles were equivalent in sciatic nerves from naïve, uninjured WT and null animals (Fig. 4*A*). Furthermore, it appeared that myelin reformation was mainly targeted, because the number of myelinated axons (Fig. 5*A*) and the axon cross-sectional area (Fig. 5*B*) remained unchanged between injured WT and $\alpha BC^{-/-}$ mice. Additional evidence in support of this notion was that the levels of GAP-43, a growth-associated protein, were equivalent in nerves from naïve and day 28 post-injured sciatic nerves from WT and null mice (Fig. 5*C*). As well, the growth of neurites (outgrowth, number of processes, and longest neurite) from cultured dorsal root ganglion (DRG) neurons was similar between the two genotypes (Fig. 5*D*). Therefore, $\alpha BC^{-/-}$ mice displayed defects in remyelination after injury and possibly not growth of axons, suggesting that Schwann cells may be specifically impacted by the loss of the heat shock protein.

αBC Regulates Differentiation of Myelinating Schwann Cells. To identify the cellular mechanism(s) underlying the remyelination deficit in injured αBC-deficient mice, the phenotype of Schwann cells was determined by quantifying the numbers of profiles in the distal nerve segment that were $S100^+$ (pan-Schwann cell marker), $GFAP^+$ (marker of dedifferentiated or nonmyelinating Schwann cells), and $P0^+$ (myelinating Schwann cells). Although the number of $S100^+$ profiles was equivalent between the WT and $\alpha BC^{-/-}$ groups from 3 to 28 d postcrush (Fig. 6*A*), the proportions of $GFAP^+$ and $P0^+$ counts were markedly different between the two genotypes. Specifically, $\alpha BC^{-/-}$ animals had fewer numbers of $P0^+$ profiles at 21 d postinjury and more $GFAP^+$ cells at 28 d postcrush compared with crushed WT nerves (Fig. 6 *B* and *C*). No differences in GFAP and P0 counts were seen at the earlier time points (3, 5, 7, and 14 d), suggesting that Schwann cell dedifferentiation and proliferation were unaffected by αBC. We then measured for levels of Krox-20, a promyelinating transcription factor in Schwann cells, and found that damaged nerves from αBC-deficient mice displayed a trend for reduced levels of Krox-20 relative to WT cohorts (Fig. 6*D*). Together, these data imply that there may be a defect in the ability of $\alpha BC^{-/-}$ dedifferentiated Schwann cells to switch back to a myelinating phenotype on contact with regenerated axons.

NRG 1–ErbB2–AKT Axis Is Modulated by αBC During Axonal Degeneration. To assess for the molecular mechanisms driving αBC actions after PNS injury as well as ascertain whether early injury processes were impacted by the crystallin, the expression of

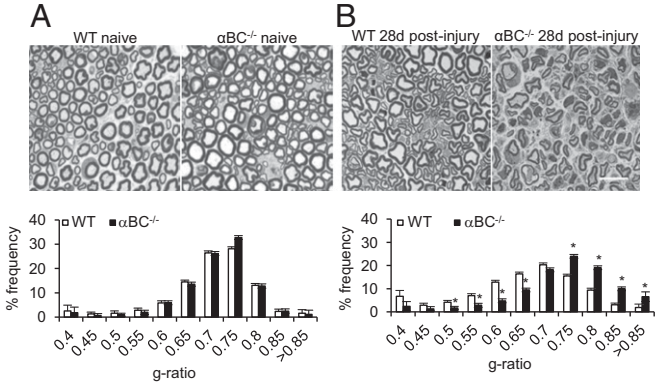

Fig. 4. Remyelination in WT and $\alpha BC^{-/-}$ mice after sciatic nerve injury. Bright-field images of toluidine blue-stained, Epon-embedded sciatic nerve cross-sections and g-ratio analyses in (*A*) naïve and (*B*) 28-d postinjured WT (white bars) and $\alpha BC^{-/-}$ (black bars) mice (representative of two experiments; $n = 3–5$ per group). Data are displayed as g-ratio frequency distribution of WT and $\alpha BC^{-/-}$ mice and analyzed using an independent *t* test. (Magnification: 100×; scale bar: 10 μm.) $^*P < 0.05$.

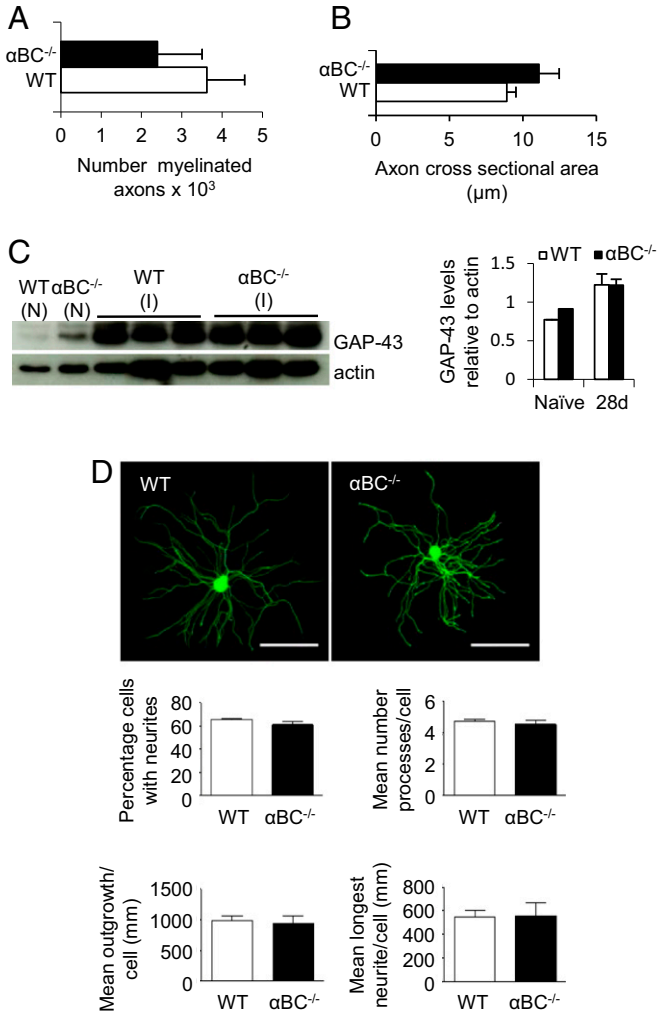

Fig. 5. Axonal characteristics of WT and αBC$^{-/-}$ mice. (*A*) Number of myelinated axons and (*B*) axon cross-sectional area in WT and αBC$^{-/-}$ mice in 28-d postcrushed Epon-embedded sections stained with toluidine blue (representative of two experiments; n = 3–5 per group). (*C*) Western blot image and ImageJ quantification of the levels of GAP-43 in naïve (N) and 28-d postinjured (I) sciatic nerves from WT (white bars) and αBC$^{-/-}$ (black bars) mice (one experiment; n = 3 per group). (*D*) Outgrowth of processes from DRGs isolated from WT and αBC$^{-/-}$ mice at 24 h in culture analyzed for percentage of cells with neurites, mean number of processes per cell, mean outgrowth per cell, and mean longest neurite per cell. Outgrowth measures were compared using the independent t test (unpaired two-tailed), with statistical significance set at $P < 0.05$. (Scale bar: 200 μm.)

neuregulin (NRG) 1 Types I and III and its receptor ErbB2 was assessed. NRG 1–ErbB signaling is involved in many postinjury events, including de- and remyelination (30, 31), Schwann cell de- and redifferentiation (31, 32), Schwann cell proliferation (33), remyelination (31), regeneration (30), and neuromuscular junction reinnervation (30). As reported previously in injured WT animals (31), the levels of neuregulin 1 Type I increased after injury (within 3 d) before decreasing back to naïve levels by 7 d postcrush (Fig. 7*A*). A similar temporal pattern was also seen in the αBC$^{-/-}$ mice (Fig. 7*A*), implying that this Schwann cell-derived neuregulin (31) is not involved in αBC-mediated injury processes. For neuregulin 1 Type III, its level decreased within 3 d after injury in WT animals and then, rebounded to baseline status at 7 d postcrush (Fig. 7*A*). This reduction, however, was minimal in the damaged null animals (Fig. 7*A*), suggesting that this axon-specific neuregulin (31) was not responding appropriately to the injury. There is thus an axonal alteration in injured αBC$^{-/-}$ mice in terms of NRG 1 Type III expression, but this change did not impact number of myelinated axons, DRG process outgrowth, or GAP-43 levels (Fig. 5). Regarding NRG 1 receptors, we assessed for the levels of phosphorylated and nonphosphorylated ErbB2. No difference was seen in the levels of nonphosphorylated ErbB2 between WT and null mice at 3, 5, 7, and 21 d after injury, whereas higher levels were observed in the naïve and 28-d injured null animals (Fig. 7*B*). With respect to phospho-ErbB2 (p-ErbB2), no expression was visible in nerves from naïve WT and αBC$^{-/-}$ mice, but there was a robust increase in both WT and null animals within 3 d of crush injury. This enhancement in p-ErbB2 was maintained until day 28 in injured WT, with a reduction evident midway at days 7 and 21 (Fig. 7*B*). A similar pattern of p-ErbB2 expression was seen in the αBC$^{-/-}$ animals but with an intriguing transient return to naïve levels 7 d after injury. Taken together, these findings indicate that αBC is involved in regulating NRG 1 Type III–ErbB2 signaling in the early period after PNS injury.

To delineate further the signal transduction pathway(s) that may be mediating the differences seen in NRG 1 Type III and p-ErbB2 in injured αBC$^{-/-}$ mice, we assessed for JNK, p38, ERK, and AKT, pathways that have been associated with PNS regeneration, Schwann cell properties, and αBC function (34–37). The levels of p-JNK, p-p38, and p-ERK1/2 were significantly up-regulated after injury in both WT and αBC$^{-/-}$ mice relative to uninjured animals, but there was no difference between the two genotypes postcrush (Fig. S3). With respect to AKT signaling, constitutive levels of AKT and p-AKT were present but were not different between uninjured WT and null nerves (Fig. 7*C*). In WT animals after damage, p-AKT expression remained similar to naïve levels until day 5, after which there was an almost complete loss of the transduction factor

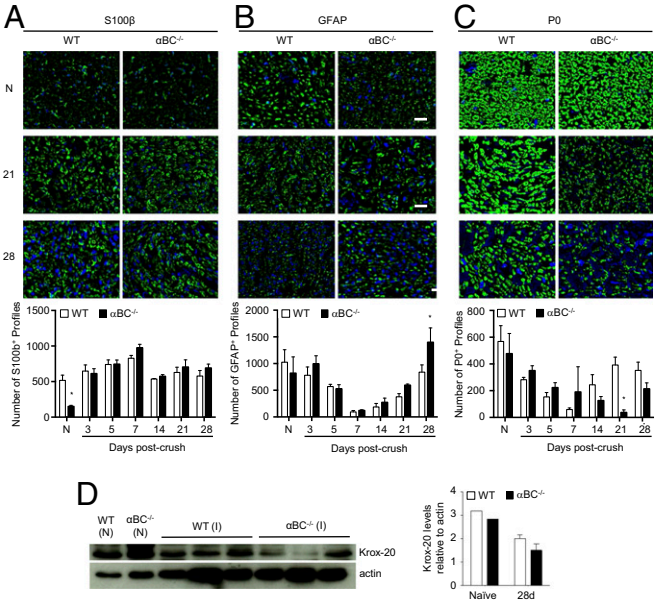

Fig. 6. Schwann cell profile in injured WT and αBC$^{-/-}$ animals. Representative images and quantification of the number of (*A*) S100^{+}, (*B*) GFAP^{+}, and (*C*) P0 profiles in the sciatic nerves of naïve (N) and 28-d postcrushed WT (white bars) and αBC$^{-/-}$ (black bars) animals (representative of two experiments; n = 3–5 animals per group). (*D*) Western blot image and ImageJ quantification of the levels of Krox-20 in naïve (N) and 28-d postinjured (I) sciatic nerves from WT (white bars) and αBC$^{-/-}$ (black bars) mice (one experiment; n = 3 per group). All data represent mean ± SEM. *$P < 0.05$ (independent t test).

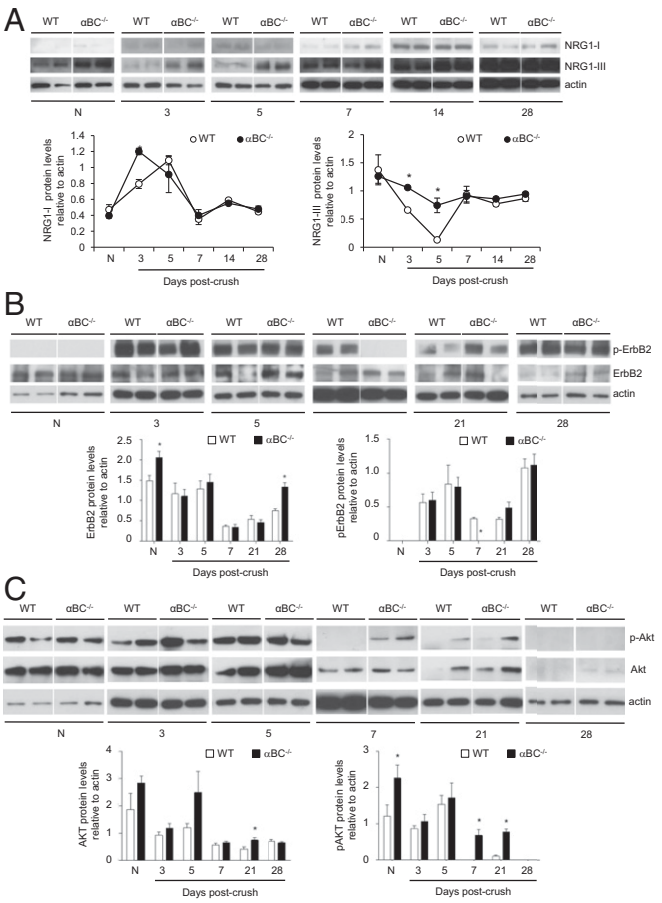

Fig. 7. Expression of neuregulin, ErbB2, and AKT in injured sciatic nerves from WT and αBC$^{-/-}$ mice. Western blot levels and ImageJ analysis of (*A*) neuregulin 1 Types I and III, (*B*) ErbB2, and (*C*) AKT in WT and αBC$^{-/-}$ animals before injury (N) and at various time points (3, 5, 7, 14, and 28 d) after crush damage (one experiment; $n = 4$ per group). Displayed are two animals per time point, with each quantification time point consisting of four animals. All data represent mean ± SEM. *$P < 0.05$ (independent *t* test).

from days 7 to 28 postcrush. In αBC$^{-/-}$ animals, p-AKT levels at days 3 and 5 postcrush also remained similar to naïve levels. However, unlike the WT cohort, lower but detectable levels of p-AKT were still evident at days 7 and 21 postcrush, and it was not until day 28 when the transduction factor was almost completely absent, like in the WT animals. For both WT and αBC$^{-/-}$ mice, AKT levels after injury remained similar to those for naïve animals at days 3 and 5 postcrush and reduced from days 7 to 28, but there was no overall difference between the two genotypes (Fig. 7*C*). Taken together, these findings indicate that αBC is involved in regulating NRG 1 Type III–ErbB2 and p-AKT signaling in the early period after PNS injury.

Exogenous Administration of αBC Is Therapeutic After Sciatic Nerve Injury. Finally, inspired by our identified PNS protective properties of αBC, we evaluated whether αBC could be therapeutic after peripheral nerve crush injury. Because the levels of endogenous αBC took several weeks to recover to baseline status after injury (Fig. 1*C*), we reasoned that exogenous application of the heat shock protein would enhance recovery processes. WT animals were injected every other day starting at day 1 after crush damage with either saline or rhu-αBC. At 28 d postdamage, animals were subjected to behavioral testing, and their nerves were assessed for remyelination by g-ratio analysis. In terms of remyelination, mice injected with rhu-αBC displayed a skewing toward low g-ratios values, which is indicative of thicker myelin sheaths. Specifically, the frequencies of axons with small (thick myelin sheaths) and large (thinner myelin thickness) g ratios were higher and lower, respectively, in the crystallin-treated group relative to controls (Fig. 8*A*). With respect to functional recovery, injured WT mice treated with rhu-αBC displayed an SFI difference of 16.42 ± 2.63 at 28 d postcrush, whereas the phosphate buffered saline (PBS) group was calculated at 50.09 ± 4.06 (Fig. 8*B*). These data indicated that walking

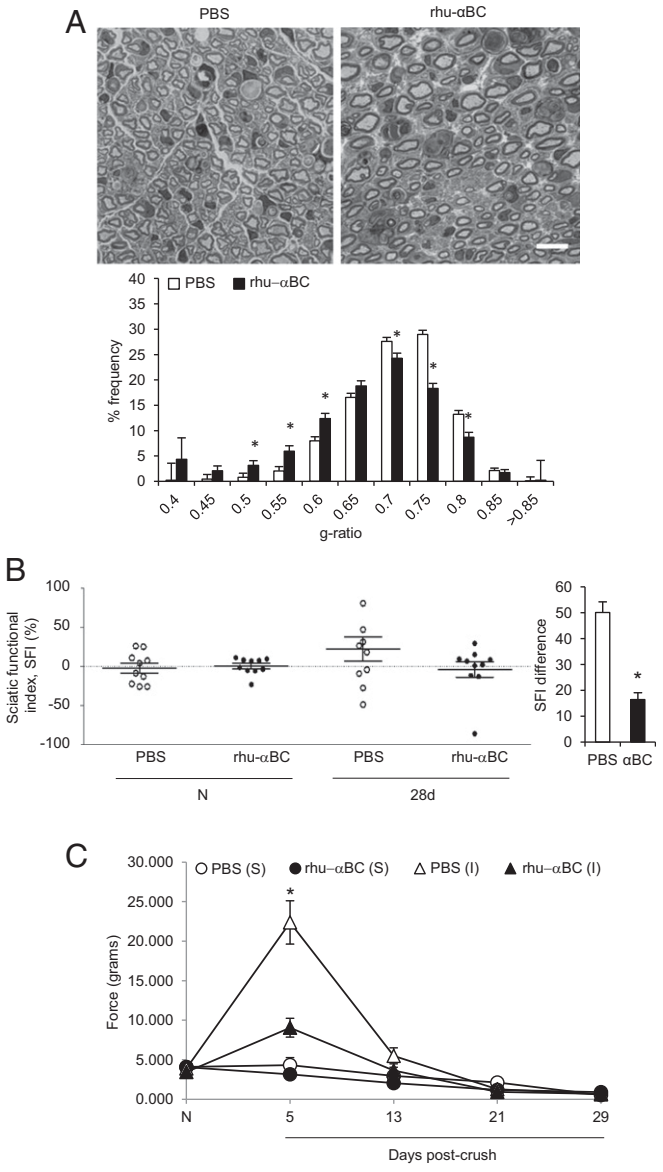

Fig. 8. Therapeutic effect of rhu-αBC in WT mice after sciatic nerve crush injury. (*A*) Representative images of toluidine blue-stained, Epon-embedded sections and g-ratio analysis from WT animals treated with PBS (white bars) or rhu-αBC (black bars) at 28 d postcrush ($n = 3$–4 per group). (Magnification: 100×; scale bar: 10 μm.) (*B*) SFI examination and SFI difference in PBS- (white circles and bar) and rhu-αBC–treated (black circles and bar) injured WT mice before [naïve (N)] and 28 d after crush injury (representative of two experiments; $n = 9$–10 mice per group). All data represent mean ± SEM. *$P < 0.05$ (independent *t* test). (*C*) von Frey Hair test in PBS- (white circles and triangles) and rhu-αBC–treated (black circles and triangles) sham (S) and injured (I) WT animals tested before [naïve (N)] and after crush (I) (one experiment; $n = 10$ mice per group). Data were analyzed using two-way repeated measures ANOVA and represent mean ± SEM. *$P < 0.05$.

ability had returned to almost preinjury status at 28 d postdamage for WT animals treated with rhu-αBC compared with the PBS cohort. The von Frey test was additionally implemented to test for mechanical sensitivity. Here, both the PBS and αBC groups showed an augmentation in force at day 5 postcrush compared with the sham cohorts that then returned to baseline levels by day 13 postdamage (Fig. 8*C*). However, the force needed to elicit a response was significantly lower in the rhu-αBC–treated group relative to the PBS-injected mice at day 5. Sensitivity early after sciatic nerve injury has been attributed to saphenous nerve sprouting in the medial and central areas of a mouse's paw (38), and thus, axon sprouting may be enhanced with exogenous application of rhu-αBC.

Discussion

Heat shock proteins have been shown to be important for recovery after PNS and CNS nerve injury. Ma et al. (39) noted that Hsp27 promoted motor recovery after sciatic nerve damage, whereas i.v. administration of rhu-αBC was shown to reduce lesion size and neuronal death and improve behavioral function after spinal cord injury (25). Because αBC is expressed in Schwann cells and axons (16–18), our study aimed to determine whether the heat shock protein plays a role in the PNS. We show that αBC modulates some postinjury processes after PNS damage. Based on the rapid reduction in expression of the crystallin within 1 d of sciatic nerve crush damage and its reup-regulation starting at 28 d postcrush (Fig. 1*C*), we hypothesized that αBC was a negative regulator of the early events, such as axon degradation, Schwann cell dedifferentiation, and Schwann cell proliferation, and/or alternately, as a positive modulator of regeneration and remyelination. We show that αBC contributes to remyelination of peripheral axons, because its absence attenuated myelin formation after crush injury. We propose that the remyelination defect is caused by a reduced ability of dedifferentiated Schwann cells to switch back to a myelinating phenotype after axon regeneration because of the reduced numbers of $P0^+$ profiles and increased presence of $GFAP^+$ cells in damaged nerves from $\alpha BC^{-/-}$ mice relative to their WT counterparts. This inability of Schwann cells to redifferentiate may be driven by disruptions in NRG 1 Type III–ErbB2 signaling seen early after PNS damage in the null animals (Fig. 7). As one would expect with deficits in remyelination, defects in the electrophysiological properties of remyelinating axons (Fig. 3) were noted in injured $\alpha BC^{-/-}$ animals that likely contributed to the observed impairments in motor and sensory behaviors in the null mice (Fig. 2). Our data also indicate that the dysfunctions in remyelination, behavior, and electrophysiological properties in injured $\alpha BC^{-/-}$ animals may not be related to defective axon regeneration, because no differences in DRG neurite outgrowth, number of myelinated axons, or levels of GAP-43 were seen between injured WT and $\alpha BC^{-/-}$ mice. It is, however, possible that axon regrowth starts slowly after injury in the null animals and then, accelerates to "catch up" with WT mice at day 28 postcrush, or vice versa, it starts fast and then, slows down, both of which could impact remyelination. Finally, we showed that αBC has therapeutic potential, because injections of rhu-αBC in injured WT animals enhanced remyelination and functional recovery after crush injury in WT animals (Fig. 8). Because of the reduced force needed to elicit a sensory response in injured animals treated with rhu-αBC at day 5 postcrush (Fig. 8*C*), it is possible that this is caused by enhanced axonal sprouting by the saphenous nerve shown by Cobianchi et al. (38) after sciatic nerve injury. We will address this possibility in a future study.

PNS Postinjury Processes. After PNS damage, an exquisitely orderly but overlapping sequence of processes occurs, in which alterations of early events (axon degeneration, Schwann cell dedifferentiation, demyelination, Schwann cell proliferation and migration, and immune cell infiltration) can impact later occurring functions, such as axon regeneration, Schwann cell redifferentiation, remyelination, and neuromuscular junction reinnervation. For example, in the Ola/WLD^s mouse, in which axon degeneration is delayed by about 2 wk, regeneration is impaired, although axon degeneration eventually occurs (40). This inadequate axon regrowth led to the suggestion that, although regeneration would eventually proceed, albeit slowly, a rapid course of Wallerian degeneration is necessary if axons are to regenerate at optimal rates and maximum extent (41). More recently, Niemi et al. (42) found that, in addition to delayed Wallerian degeneration, reduced PNS regeneration in injured Ola animals seems to be related to defects at the level of the neuronal cell body, because neurite outgrowth is impaired if macrophages and their products are reduced or absent. This idea of early PNS injury events impacting later processes extends to other functions, such as Schwann cell redifferentiation and remyelination. A number of seminal studies showed that early upregulation of the MAP kinases (MAPKs), c-Jun (37), ERK (35), and p38 (36) in Schwann cells after injury drove dedifferentiation and proliferation of these glial cells and that prolonging or eliminating their presence markedly altered myelin clearance, regeneration, and remyelination. In addition, suppression or loss of NRGs or ErbBs, which drives multiple aspects of Schwann cell and axon biology after injury, such as de- and remyelination (31, 43), Schwann cell de- and redifferentiation (31, 32), regeneration (30), and neuromuscular junction reinnervation (30), disrupts regeneration and remyelination (31).

Our work suggests that the defect in remyelination (Fig. 4) and possible inability of dedifferentiated Schwann cells to redifferentiate (Fig. 6) in injured null mice are related to alterations in early injury events in the $\alpha BC^{-/-}$ mice. Evidence in support of this idea is that expression of NRG 1 Type III, which normally declines after PNS injury (31), remains elevated in the knockout animals after injury (Fig. 7*A*). We speculate that the axons have not recognized that an injury has occurred and as a consequence, respond inappropriately by maintaining constitutive NRG 1 Type III expression—we indeed show that Wallerian and Wallerian-like processes, such as neurofilament degeneration, myelin clearance, and macrophage infiltration, are occurring at equivalent levels in both injured WT and null mice (Fig. S4). The unchanged NRG 1 Type III levels in the $\alpha BC^{-/-}$ animals likely impact later processes, because a reduction in NRG 1 Type III initiates events, such as Schwann cell dedifferentiation and demyelination (31). Furthermore, the transient near absence of ErbB2 expression at day 7 postcrush in the null mice could also impact later remyelination. As reported by others (44), we see an increase in expression of ErbB2 after sciatic nerve crush in WT animals, but there was an interesting biphasic pattern in the WT animals, where levels dipped at day 7 postcrush before rebounding at day 28. The dual temporal responses could imply a switch in functions for ErbB2. That is, the first increase could be related to early Schwann cell functions, such as proliferation, and the second could be related to later events, like remyelination. Guertin et al. (45) also reported a biphasic response for ErbB2, where a transient increase in the first hour of peripheral nerve damage was associated with demyelination, whereas a later increase around day 3 was associated with remyelination. In our $\alpha BC^{-/-}$ mice, a similar biphasic response was evident, but the transient loss of p-ErbB2 at day 7, although NRG 1 Type III levels had returned to baseline, could deviate the course of Wallerian degeneration and thus, negatively impact later events that p-ErbB2 is involved in, such as remyelination and redifferentiation. Some reported evidence in support of this idea is that the density of ErbBs appears to modulates NRG 1 activity and that its absence can render Schwann cells insensitive to axonal NRG 1 (32). Along the same lines, axonal NRG 1 Type III appears to act in a concentration-dependent manner, whereby Schwann cells display distinct responses, promyelination, or myelin inhibition depending on the levels of the NRG (32, 46).

Thus, changes in either NRG 1 Type III or ErbB2 would disrupt the communication between injured axons and Schwann cells and the many downstream processes that they regulate, such as remyelination. With respect to other properties of Schwann cells, our data suggest that Schwann cell dedifferentiation and proliferation are not impacted by αBC, because the numbers of $P0^+$ and $GFAP^+$ profiles are equivalent between WT and null animals at all time points. There thus seems to be selectivity in the function of the heat shock protein after PNS damage.

Signal Transduction Signaling During Axonal Degeneration. In an effort to identify the molecular mechanism(s) underlying the axonal degeneration changes in $\alpha BC^{-/-}$ animals, we assessed for MAPK and AKT signaling. The many reported functions of αBC, such as cell survival, immunosuppression, and chaperoning, involve the JNK, p38, and ERK pathways (21, 22, 47, 48). These signaling factors also participate in various aspects of Schwann cell function after peripheral nerve damage, including Schwann cell dedifferentiation and proliferation, regeneration, Schwann cell differentiation, and remyelination (34–37). We found that MAPKs were not altered before and after injury in the null mice compared with WT counterparts, indicating that these signal transduction factors do not universally mediate all functions of the heat shock protein. Rather and unexpectedly, we discovered that the AKT pathway was associated with αBC function after peripheral nerve damage. The PI3K-AKT pathway has been implicated in PNS remyelination (34), whereby increased levels or deficiency promoted or inhibited both PNS and CNS myelination (34). However, recent work by Heller et al. (49) noted that the PI3K pathway, which can act via AKT, has differing effects on Schwann cell myelination depending on its temporal expression. Early presence was associated with myelination via AKT/mTOR, but later expression via laminin activation negatively affected myelination. In our model system, we did not observe an increase in AKT after injury. Rather, an almost complete absence was clearly evident from day 7 postcrush in WT animals, whereas expression of the signal transduction factor was prolonged until much later at day 28 in the null animals. It is possible that the prolonged presence of AKT in the injured $\alpha BC^{-/-}$ animals negatively influenced remyelination similar to that seen in the study by Heller et al. (49).

Finally, in addition to remyelination, it is also possible that αBC may be involved in triggering the degeneration process after PNS injury. In 2011, Wakatsuki et al. (50) showed that degradation of p-AKT levels was required for normal axon degeneration to occur after PNS injury. Breakdown of p-AKT releases inactivation of GSK3, which allows for phosphorylation of CRMP2 that is needed for microtubule reorganization (50). Thus, like WLD^s mice, the pronounced delay in reduction of p-AKT until day 28 after crush damage in $\alpha BC^{-/-}$ animals could negatively impact later postinjury processes, like Schwann cell redifferentiation and remyelination.

Conclusion

In summary, this study shows that αBC regulates specific events after damage to the PNS in the PNS. We show that Schwann cell redifferentiation and remyelination are regulated by αBC after peripheral nerve injury and that these processes may be impacted by the heat shock protein also modulating events in the early phase of axonal degeneration, such as NRG 1 Type III–ErbB2-AKT signaling and possibly, degeneration.

Materials and Methods

Mice. $\alpha BC^{-/-}$ mice were developed at the NIH National Eye Institute (51). The animals were generated from ES cells with a 129S4/SvJae background and maintained in 129S6/SvEvTac × 129S4/SvJae background. $\alpha BC^{-/-}$ mice are viable and fertile, with no obvious prenatal defects and normal lens transparency. Older mice show postural defects and progressive myopathy that are apparent at ∼40 wk of age (51). We studied these animals between 8–12 wk, thus removing the possible effects of myopathy on our behavioral evaluation. Furthermore, we performed analyses on age-matched uninjured 129S6/SvEvTac WT and $\alpha BC^{-/-}$ before injury to confirm equivalent baseline properties. Colonies of WT and $\alpha BC^{-/-}$ mice were bred and maintained in our animal facility that maintains a 12-h light/12-h dark cycle. Mice are housed at a maximum of five animals per cage. All procedures were carried out in accordance with guidelines of the Canadian Council of Animal Care and have received approval from the University of Calgary Animal Resources and Ethics Committee.

Surgery. Eight- to 12-wk-old female WT and $\alpha BC^{-/-}$ mice were anesthetized with a 3:1 ketamine:xylazine (200 mg/kg:10 mg/kg) mixture by i.p. injection. An incision was made through the skin below the hip, and the muscle was blunt dissected using fine surgical scissors and forceps to expose the right sciatic nerve at midthigh level. The nerve was crushed 0.5 cm above the region where it splits into the sural, common peroneal, and tibial branches. For crushing, the sciatic nerve was first compressed with a straight tip serrated 5.0 fine forceps for 30 s. To ensure that the majority of axons were damaged, the forceps were then rotated 90°, and the same area was crushed again for an additional 30 s until a translucent region was evident. Evidence that the majority of axons sustained injury is shown in Fig. S5, where high expression of NF-H that is typically seen in intact nerves was markedly reduced in damaged fibers particularly at and around the crush site. Also, punctate, irregular NF staining distal to the crush site was observed that is likely axonal debris (Fig. S5*D*). Animals were allowed to recover on a heated pad and killed at 1, 3, 5, 7, 14, 21, 28, or 56 d postinjury. Naïve represents mice that have not undergone any surgical manipulation, whereas sham refers to undamaged nerves on the contralateral side of unilaterally crushed mice, where only the skin and muscles overlying the sciatic notch area were incised.

Western Blotting. In total, 30–50 μg total protein was subjected to 5–15% sodium dodecyl sulfate polyacrylamide gel electrophoresis (SDS/PAGE), transferred to polyvinylidene fluoride (PVDF) membranes, and blocked with 5% (wt/vol) nonfat dried milk in Tris·hydrochloride (HCl)-buffered saline containing 0.05% Tween-20. Membranes were immunoblotted overnight at 4 °C with the following primary antibodies: Ms anti–GAP-43 (MAB347; 1:400; Millipore), Rb anti-αBC (ABN185; 1:1,000; EMD Millipore), Rb anti-actin (A2066; 1:1,000; Sigma-Aldrich), Rb neuregulin 1 Type I (sc-348; 1:500; Santa Cruz), Ms neuregulin 1 Type III (MABN42; 1:1,000; Millipore), Sh ErbB2 (AF5176; 1:1,000; R&D), Ms p-ErbB2 (04–294; 1:1,000; Millipore), Rb AKT (9272; 1:1,000; Cell Signaling), Rb p-AKT (4060; 1:1,000; Cell Signaling), Rb p38 (9212; 1:1,000; Cell Signaling), Ms p-p38 (9216; 1:2,000; Cell Signaling), Rb ERK (9102; 1:1,000; Cell Signaling), Rb p-ERK (9101; 1:1,000; Cell Signaling), Rb JNK (9252; 1:1,000; Cell Signaling), and Rb p-JNK (9251; 1:1,000; Cell Signaling). Bound primary antibodies were visualized with horseradish peroxide (HRP)-conjugated anti-rabbit IgG, anti-mouse IgG (1:5,000; GE Healthcare), or anti-sheep IgG (1:1,000; R&D) followed by chemiluminescence detection using an electrochemiluminescence (ECL) Kit (Pierce).

Immunohistochemistry. Sciatic nerves were fixed in Zamboni's fixative, cryoprotected in 30% (wt/vol) sucrose solution, and frozen; 10-μm-thick sections were blocked with 0.1% Triton X-100 and 10% (vol/vol) normal goat serum followed by overnight incubation at 4 °C with the following primary antibodies: Rb anti-αBC (ABN185; 1:200; Chemicon), Ms anti-total–NF-H (2836; 1:400; Cell Signaling), Ms anti-MBP (SMI94; 1:500; Covance), Rb anti-GFAP (Z0334; 1:500; DAKO), Rb anti-myelin protein P0 (ABN363; 1:200; Millipore), Ms anti-Asma (A5228; 1:200; Sigma-Aldrich), Rt anti-F4/80 (MCA497EL; 1:200; AbD Serotec), Ms anti–non-p–NF-H (SMI-32R; 1:200; Covance), Rb anti–Iba-1 (019–19741; 1:200; Wako Chemicals), Ms anti-S100 (S2532; 1:500; Sigma-Aldrich), and DAPI (D3571; 1:2,000; Invitrogen). Bound antibody was detected using the following Invitrogen secondary antibodies at 1:200: anti-mouse 594 (A11005), anti-mouse 488 (A11007), anti-rabbit 594 (A11012), and anti-rabbit 488 (A11008).

Remyelination and g-Ratio Analysis. Sciatic nerves were removed and immersed in 2.5% gluteraldehyde in 0.1 M cacodylate buffer, pH 7.4, at 4 °C overnight. Nerves were then postfixed in 2% (vol/vol) osmium tetroxide in 0.1 M cacodylate buffer, pH 7.4, for 2.5 h at room temperature and embedded in Epon after alcohol dehydration. Semithin sections were stained with toluidine blue. Sections were examined on an Olympus BX51 Upright Microscope at 100× magnification; g ratios of the images were analyzed using the ImageTrak software created by P. K. Stys (www.ucalgary.ca/styslab/imagetrak). The g ratios of seven areas of each sciatic nerve were analyzed. Using the Autotrace Polygon Tool to identify myelinated axons, measurements of the inner area (axon), outer area (total fiber), and g ratio were computed.

The g ratio is obtained by dividing the diameter of an axon by the diameter of the axon plus myelin sheath. Thus, a low g ratio signifies thickly myelinated axons, whereas fibers with thin myelin sheaths have a large g ratio. The analyzer was masked to the genotypes during quantification.

DRG Neuron Isolation, Staining, and Quantification.

i) Isolation. L4–L6 DRGs were digested in a 0.1% collagenase/L15 solution for 60 min at 37 °C. Debris was removed by density gradient centrifugation (100 × *g* for 6 min), and cells were resuspended in Dulbecco's modified Eagle medium (DMEM)/F12. Neurons were plated in triplicate on a glass substrate coated with poly–L-lysine (0.01%) and mouse laminin (10 μg/mL) and allowed to adhere for 10 min followed by the addition of culture medium. Cells were then incubated at 37 °C in 5% CO_2 for 18 h.

ii) Staining. Cultured neurons were fixed in 37 °C 4% (wt/vol) paraformaldehyde (PFA)/1× PIPES Hepes EGTA $MgSO_4$ (PHEM) buffer, blocked with 5% (vol/vol) goat serum/1× PBS (20 min), and labeled with a primary antibody mixture of Ms anti-NF200 (N0142; 1:800; Sigma-Aldrich) and Ms anti–βIII-tubulin (801201; 1:1,000; BioLegend) to visualize neurites. Bound antibody was detected using the secondary antibody Alexa 488 (A11001; 1:200) and then, mounted on a glass slide using Vectashield mounting medium with DAPI nuclear stain. Neurite outgrowth was quantified using the Neurite Outgrowth function of the MetaXpress (Molecular Devices) software.

Electrophysiological Assessment. Normalized distal motor latencies and MNCV were performed in naïve and 28-d postinjury animals. For normalized distal motor latencies, the sciatic nerve was stimulated just above the sciatic notch using bipolar hook electrodes and the electromyogram activity was recorded (100×; 100 Hz to 1 kHz) using bipolar recording electrodes inserted into the first dorsal interosseous muscle of the corresponding hind limb. The latency to record a compound muscle action potential (CMAP) from the dorsal interosseus muscle is called the distal latency. The conduction delay was measured from the onset of the stimulus artifact to the upward deflection of the CMAP. Normalized distal motor latencies were calculated by dividing the latencies by the distance from the stimulation to the recording site. These latencies depend on distal motor axon conduction velocity, neuromuscular transmission delay, and muscle activation. The experimenter was masked to the genotypes during recording.

To calculate MNCV, both the sciatic notch and knee (popliteal fossa) were stimulated, and the CMAPs were recorded from the tibial-innervated dorsal interossei foot muscles using subdermal needle electrodes. Conduction velocity of the nerve was calculated by dividing the difference in distance between the knee and the sciatic notch knee stimulating site by the difference in the latencies of the respective CMAPs. CMAP amplitudes were measured from baseline to peak and taken as the average value from the two stimulation sites. The body temperature of animals was kept constant at 37 °C ± 0.5 °C throughout the experiment using a heating lamp (52).

Behavioral Tests. All behavioral testing was performed in the light cycle.

DigiGait. The DigiGait Imaging System (Mouse Specifics, Inc.) was used to assess gait dynamics before crush injury and 28 d postdamage (27). WT and $\alpha BC^{-/-}$ mice were placed on a motorized treadmill within a Plexiglas compartment. Digital video images were acquired at a rate of 80 frames per second by a camera mounted underneath the treadmill to visualize paw contacts on the treadmill belt. The treadmill was set at a fixed speed of 15 cm/s, which was determined as the baseline for both WT and $\alpha BC^{-/-}$ mice. The DigiGait software calculates values for multiple gait parameters, including swing duration, braking duration, propulsion duration, and paw area.

Sensory function. Before testing the behavioral responses to thermal or mechanical stimuli, mice were habituated to the test environment for 30 min. To assess thermal sensitivity (Hargreaves test), hind paw withdrawal latencies to a radiant heat lamp were determined as the average of three measurements per paw over a 30-min test period. Mechanical sensitivity was assessed using von Frey hairs ranging from 0.027 to 3.63 g. The series of von Frey hairs was applied from below the platform to the plantar surface of the hind paw in ascending order beginning with the lowest weight hair. The hair was applied until buckling occurred and then, maintained for 2 s. A trial consisted of application of the von Frey hair to the hind paw five times at 5-s intervals. If withdrawal did not occur during five applications of a particular hair, the next larger hair in the series was applied in a similar manner. The withdrawal threshold was determined as withdrawal from a particular hair four or five times of five applications. Three trials were run for each of the left (sham) and right (injured) hind paws.

Motor behavior.

i) Rotarod. Before testing, mice were left to habituate in the testing room for 30 min. Mice were trained on the rotarod for 3 d and three trials per day for a maximum time of 3 min and 5-min intertrial intervals. Mice were gently placed onto the rotarod by gently swinging the mouse by the tail onto the rotating rod. After the mice were on the rotating rod, the lever was raised to start the trial. On the first few trials, the rod was set at a low speed of 4 rpm and then, eventually increased to 12 rpm (training speed). On the day of testing, the rotarod was set to accelerating mode, which is a speed of 4–40 rpm over 5 min. The mice were placed on the rod, and the testing started after they were in place. Each mouse was given one trial for a maximum of 5 min. The latency to fall and the speed at which the mice fell for each trial were recorded.

ii) Dynamic Plantar. Before testing, mice were left to settle in the testing room for 30 min. Before the actual test, mice were given three habituation sessions—mice were placed in an overturned clear cup on a mesh grid for 15 min. On the day of testing, the Dynamic Plantar aesthesiometer was calibrated using 0-, 5-, and 50-g weights. Mice were placed in cups for 15 min on the grid until they were settled and quiet. Each mouse was given three trials on each hind paw—alternate hind paws for each trial and 5-min wait between trials. Using the mirror, the probe was directed to the center plantar surface of the paw. The latency to respond in seconds and the force in grams were recorded automatically by the Dynamic Plantar aesthesiometer.

iii) Walking track analysis/SFI. Gait was analyzed by a 4 × 6 × 50-cm corridor, in which a 50-cm-long piece of white paper was placed on its base. Nontoxic red food coloring was painted onto the hind paws of each mouse. After two practice trials, the mice walked into a covered box at the far end without hesitation. Two test trials were obtained for each mouse. Using the method described by de Medinaceli et al. (53), footprints were analyzed by the following four measurements: distance to the opposite foot, footprint length, maximal toe spreading between first and fifth toes, and paw spreading between the center of the second and fourth toes. Measurements were taken for both the normal leg and the experimental leg. An index of zero reflects normal function, and an index of ±100 theoretically represents complete loss of function.

Therapeutic Application of αBC. Uninjured 8-wk-old female WT mice underwent walking track and von Frey analysis to establish gait baselines for each mouse. Sciatic nerve crush injuries were then performed, and animals were injected with either 10 μg rhu-αBC (C7944-53; USBiologicals) diluted in 100 μL saline or 100 μL saline as control every other day starting at day 1 after surgery for 4 wk for a total of 14 injections. At the end of the treatment period, animals underwent walking track and von Frey analysis again before their nerves were processed for Epon embedding. Semithin sections were stained with toluidine blue, and g-ratio analyses were performed.

Statistical Analysis. Data are presented as means and SEMs. A two-tailed independent Student's *t* test ($n = 2$ groups) was used to detect between-group differences. ANOVA was used for $n > 2$ groups, whereas a two-way repeated measures ANOVA was implemented for repeated measures. $P < 0.05$ was considered significant.

ACKNOWLEDGMENTS. This work was supported by a seed grant from the University of Calgary University Research Grants Committee, bridge funding from Alberta Innovates–Health Solutions (AIHS) and the University of Calgary Cumming School of Medicine, and a Hotchkiss Brain Institute Axon Biology and Regeneration Theme Studentship Support Grant. E.-M.F.L. was supported by a studentship from AIHS.

1. Waller A (1850) Experiments on the section of the glossopharyngeal and hypoglossal nerves of the frog, and observations of the alterations produced thereby in the structure of their primitive fibres. *Philos Trans R Soc Lond* 140:423–429.
2. Schlaepfer WW, Bunge RP (1973) Effects of calcium ion concentration on the degeneration of amputated axons in tissue culture. *J Cell Biol* 59(2 Pt 1):456–470.
3. Stoll G, Griffin JW, Li CY, Trapp BD (1989) Wallerian degeneration in the peripheral nervous system: Participation of both Schwann cells and macrophages in myelin degradation. *J Neurocytol* 18(5):671–683.
4. Hall S (2005) The response to injury in the peripheral nervous system. *J Bone Joint Surg Br* 87(10):1309–1319.
5. Li X, Gonias SL, Campana WM (2005) Schwann cells express erythropoietin receptor and represent a major target for Epo in peripheral nerve injury. *Glia* 51(4):254–265.
6. Murinson BB, Archer DR, Li Y, Griffin JW (2005) Degeneration of myelinated efferent fibers prompts mitosis in Remak Schwann cells of uninjured C-fiber afferents. *J Neurosci* 25(5):1179–1187.

7. Pellegrino RG, Politis MJ, Ritchie JM, Spencer PS (1986) Events in degenerating cat peripheral nerve: Induction of Schwann cell S phase and its relation to nerve fibre degeneration. *J Neurocytol* 15(1):17–28.
8. Madduri S, Gander B (2010) Schwann cell delivery of neurotrophic factors for peripheral nerve regeneration. *J Peripher Nerv Syst* 15(2):93–103.
9. Gaudet AD, Popovich PG, Ramer MS (2011) Wallerian degeneration: Gaining perspective on inflammatory events after peripheral nerve injury. *J Neuroinflammation* 8:110.
10. Bhatheja K, Field J (2006) Schwann cells: Origins and role in axonal maintenance and regeneration. *Int J Biochem Cell Biol* 38(12):1995–1999.
11. Deumens R, et al. (2010) Repairing injured peripheral nerves: Bridging the gap. *Prog Neurobiol* 92(3):245–276.
12. Verdú E, Ceballos D, Vilches JJ, Navarro X (2000) Influence of aging on peripheral nerve function and regeneration. *J Peripher Nerv Syst* 5(4):191–208.
13. Terenghi G, Calder JS, Birch R, Hall SM (1998) A morphological study of Schwann cells and axonal regeneration in chronically transected human peripheral nerves. *J Hand Surg [Br]* 23(5):583–587.
14. Soilu-Hänninen M, et al. (1999) Nerve growth factor signaling through p75 induces apoptosis in Schwann cells via a Bcl-2-independent pathway. *J Neurosci* 19(12): 4828–4838.
15. Reyes O, Sosa I, Kuffler DP (2005) Promoting neurological recovery following a traumatic peripheral nerve injury. *P R Health Sci J* 24(3):215–223.
16. D'Antonio M, et al. (2006) Gene profiling and bioinformatic analysis of Schwann cell embryonic development and myelination. *Glia* 53(5):501–515.
17. Iwaki T, Kume-Iwaki A, Goldman JE (1990) Cellular distribution of alpha B-crystallin in non-lenticular tissues. *J Histochem Cytochem* 38(1):31–39.
18. Willis D, et al. (2005) Differential transport and local translation of cytoskeletal, injury-response, and neurodegeneration protein mRNAs in axons. *J Neurosci* 25(4): 778–791.
19. Rajasekaran NS, et al. (2007) Human alpha B-crystallin mutation causes oxido-reductive stress and protein aggregation cardiomyopathy in mice. *Cell* 130(3):427–439.
20. Vicart P, et al. (1998) A missense mutation in the alphaB-crystallin chaperone gene causes a desmin-related myopathy. *Nat Genet* 20(1):92–95.
21. Liu JP, et al. (2004) Human alphaA- and alphaB-crystallins prevent UVA-induced apoptosis through regulation of PKCalpha, RAF/MEK/ERK and AKT signaling pathways. *Exp Eye Res* 79(3):393–403.
22. Ousman SS, et al. (2007) Protective and therapeutic role for alphaB-crystallin in autoimmune demyelination. *Nature* 448(7152):474–479.
23. Quach QL, et al. (2013) CRYAB modulates the activation of CD4+ T cells from relapsing-remitting multiple sclerosis patients. *Mult Scler* 19(14):1867–1877.
24. Masilamoni JG, et al. (2006) Molecular chaperone alpha-crystallin prevents detrimental effects of neuroinflammation. *Biochim Biophys Acta* 1762(3):284–293.
25. Klopstein A, et al. (2012) Beneficial effects of αB-crystallin in spinal cord contusion injury. *J Neurosci* 32(42):14478–14488.
26. Cameron AA, et al. (1997) Time course of degenerative and regenerative changes in the dorsal horn in a rat model of peripheral neuropathy. *J Comp Neurol* 379(3): 428–442.
27. Berryman ER, Harris RL, Moalli M, Bagi CM (2009) Digigait quantitation of gait dynamics in rat rheumatoid arthritis model. *J Musculoskelet Neuronal Interact* 9(2): 89–98.
28. Navarro X (2016) Functional evaluation of peripheral nerve regeneration and target reinnervation in animal models: A critical overview. *Eur J Neurosci* 43(3):271–286.
29. Hildebrand C, Bowe CM, Remahl IN (1994) Myelination and myelin sheath remodelling in normal and pathological PNS nerve fibres. *Prog Neurobiol* 43(2):85–141.
30. Fricker FR, et al. (2011) Axonally derived neuregulin-1 is required for remyelination and regeneration after nerve injury in adulthood. *J Neurosci* 31(9):3225–3233.
31. Stassart RM, et al. (2013) A role for Schwann cell-derived neuregulin-1 in remyelination. *Nat Neurosci* 16(1):48–54.
32. Taveggia C, et al. (2005) Neuregulin-1 type III determines the ensheathment fate of axons. *Neuron* 47(5):681–694.
33. Carroll SL, Miller ML, Frohnert PW, Kim SS, Corbett JA (1997) Expression of neuregulins and their putative receptors, ErbB2 and ErbB3, is induced during Wallerian degeneration. *J Neurosci* 17(5):1642–1659.
34. Taveggia C (2016) Schwann cells-axon interaction in myelination. *Curr Opin Neurobiol* 39:24–29.
35. Napoli I, et al. (2012) A central role for the ERK-signaling pathway in controlling Schwann cell plasticity and peripheral nerve regeneration in vivo. *Neuron* 73(4): 729–742.
36. Yang DP, et al. (2012) p38 MAPK activation promotes denervated Schwann cell phenotype and functions as a negative regulator of Schwann cell differentiation and myelination. *J Neurosci* 32(21):7158–7168.
37. Arthur-Farraj PJ, et al. (2012) c-Jun reprograms Schwann cells of injured nerves to generate a repair cell essential for regeneration. *Neuron* 75(4):633–647.
38. Cobianchi S, de Cruz J, Navarro X (2014) Assessment of sensory thresholds and nociceptive fiber growth after sciatic nerve injury reveals the differential contribution of collateral reinnervation and nerve regeneration to neuropathic pain. *Exp Neurol* 255: 1–11.
39. Ma CH, et al. (2011) Accelerating axonal growth promotes motor recovery after peripheral nerve injury in mice. *J Clin Invest* 121(11):4332–4347.
40. Bisby MA, Chen S (1990) Delayed wallerian degeneration in sciatic nerves of C57BL/Ola mice is associated with impaired regeneration of sensory axons. *Brain Res* 530(1): 117–120.
41. Brown MC, Lunn ER, Perry VH (1992) Consequences of slow Wallerian degeneration for regenerating motor and sensory axons. *J Neurobiol* 23(5):521–536.
42. Niemi JP, et al. (2013) A critical role for macrophages near axotomized neuronal cell bodies in stimulating nerve regeneration. *J Neurosci* 33(41):16236–16248.
43. Fricker FR, et al. (2013) Axonal neuregulin 1 is a rate limiting but not essential factor for nerve remyelination. *Brain* 136(Pt 7):2279–2297.
44. Kwon YK, et al. (1997) Activation of ErbB2 during wallerian degeneration of sciatic nerve. *J Neurosci* 17(21):8293–8299.
45. Guertin AD, Zhang DP, Mak KS, Alberta JA, Kim HA (2005) Microanatomy of axon/glial signaling during Wallerian degeneration. *J Neurosci* 25(13):3478–3487.
46. Syed N, et al. (2010) Soluble neuregulin-1 has bifunctional, concentration-dependent effects on Schwann cell myelination. *J Neurosci* 30(17):6122–6131.
47. Li DW, et al. (2005) Calcium-activated RAF/MEK/ERK signaling pathway mediates p53-dependent apoptosis and is abrogated by alpha B-crystallin through inhibition of RAS activation. *Mol Biol Cell* 16(9):4437–4453.
48. Hoover HE, Thuerauf DJ, Martindale JJ, Glembotski CC (2000) alpha B-crystallin gene induction and phosphorylation by MKK6-activated p38. A potential role for alpha B-crystallin as a target of the p38 branch of the cardiac stress response. *J Biol Chem* 275(31):23825–23833.
49. Heller BA, et al. (2014) Functionally distinct PI 3-kinase pathways regulate myelination in the peripheral nervous system. *J Cell Biol* 204(7):1219–1236.
50. Wakatsuki S, Saitoh F, Araki T (2011) ZNRF1 promotes Wallerian degeneration by degrading AKT to induce GSK3B-dependent CRMP2 phosphorylation. *Nat Cell Biol* 13(12):1415–1423.
51. Brady JP, et al. (2001) AlphaB-crystallin in lens development and muscle integrity: A gene knockout approach. *Invest Ophthalmol Vis Sci* 42(12):2924–2934.
52. Kennedy JM, Zochodne DW (2005) Experimental diabetic neuropathy with spontaneous recovery: Is there irreparable damage? *Diabetes* 54(3):830–837.
53. de Medinaceli L, Freed WJ, Wyatt RJ (1982) An index of the functional condition of rat sciatic nerve based on measurements made from walking tracks. *Exp Neurol* 77(3): 634–643.